*Article*

# Broadening the Photoluminescence Excitation Spectral Bandwidth of YVO$_4$:Eu$^{3+}$ Nanoparticles via a Novel Core-Shell and Hybridization Approach

**Jianhua Huang** [1,2,†], **Lu Tang** [1,3,†], **Nan Chen** [1,*] **and Guoping Du** [1,*]

[1] School of Materials Science and Engineering, Nanchang University, Nanchang 330031, China
[2] Hunan Engineering Laboratory for Control and Optimization of PV Systems, Hunan Vocational Institute of Technology, Xiangtan 411104, China
[3] The Center of Collaboration and Innovation, Jiangxi University of Technology, Nanchang 330098, China
[*] Correspondence: nanchen@ncu.edu.cn (N.C.); guopingdu@ncu.edu.cn (G.D.)
[†] Jianhua Huang and Lu Tang contributed equally to this article.

check for updates

**Abstract:** For many optoelectronic applications, it is desirable for the lanthanide-doped phosphors to have broad excitation spectrum. The excitation mechanism of the lanthanide-doped YVO$_4$, a high quantum efficient lasing material, primarily originates from the energy transfer process from the host VO$_4^{3-}$ complexes to the lanthanide ions, which has an excitation spectral bandwidth range of 230–330 nm. For applications in silicon solar cells, such phosphors can convert ultraviolet light to visible light for more efficient power generation, but this spectral range is still not broad enough to cover the entire ultraviolet spectrum of solar light. In this work, a novel core-shell and inorganic–organic hybridization strategy has been employed to fabricate Eu$^{3+}$-doped YVO$_4$ nanoparticles to broaden their photoluminescence excitation spectral bandwidth to the range of 230–415 nm, covering the entire ultraviolet spectrum of solar light and enabling their potential applications in silicon solar cells.

## 1. Introduction

Lanthanide ion-doped YVO$_4$ (YVO$_4$:Ln$^{3+}$), such as YVO$_4$:Nd$^{3+}$, has been widely used for fabricating lasers [1,2]. Recently, luminescent YVO$_4$:Ln$^{3+}$ nanomaterials, such as YVO$_4$:Eu$^{3+}$ [3,4], YVO$_4$:Eu$^{3+}$,Bi$^{3+}$ [5,6], YVO$_4$:Yb$^{3+}$ [7], YVO$_4$:Yb$^{3+}$,Bi$^{3+}$ [8] etc., have received extensive attention for enhancing the conversion efficiency of solar cells. Solar cells, especially the silicon solar cells, usually have rather low quantum efficiency in the ultraviolet (UV) spectrum, but, in the visible/near infrared spectrum, however, their quantum efficiency is quite high. YVO$_4$:Ln$^{3+}$ nanomaterials are excited by UV lights of solar irradiance, and down-convert them to visible or near infrared lights. Through such down-conversion, the conversion efficiency of solar cells is consequently enhanced as a result of more efficient utilization of UV photons of solar irradiance [9,10].

The strong photoluminescence of YVO$_4$:Ln$^{3+}$ relies on the efficient energy transfer process from the host VO$_4^{3-}$ complexes to the Ln$^{3+}$ [11], in which the VO$_4^{3-}$ is well excited by the UV lights. Such an energy transfer process effectively overcomes the drawback of low absorption cross sections of parity forbidden 4f–4f transitions of Ln$^{3+}$ ions. The excitation spectrum of VO$_4^{3-}$ peaks at about 325 nm, and has a spectral range from 260 nm to 330 nm at the half maximum and a band edge at 350 nm [12]. This, however, is too narrow to cover the UV spectrum (250–400 nm) of the solar lights on earth surface

for applications in solar cells. To extend its excitation spectrum, $Bi^{3+}$ ions have been co-doped into $YVO_4$:$Ln^{3+}$ [5,6,8,13,14]. It was found that the peaking wavelength of its excitation spectrum is shifted to the longer wavelength at 342 nm and the band edge is extended to about 360 nm [8]. Up to now, however, the excitation bandwidth of $YVO_4$:$Ln^{3+}$ is still not wide enough to cover the UV spectrum of the solar irradiance. Previous work on $LaF_3$:$Eu^{3+}$ [15] has shown that its excitation spectral bandwidth can be effectively broadened by using a mixed photoluminescence sensitization from different types of organic ligands.

In this work, a novel strategy was employed to remarkably broaden the excitation spectrum of $YVO_4$:$Eu^{3+}$ nanoparticles through a dual–channel excitation approach, and the entire UV spectrum of the solar irradiance can be effectively covered. This was implemented by combining the two strong excitation channels, the efficient $VO_4{}^{3-} \rightarrow Eu^{3+}$ energy transfer after annealing and the photoluminescence sensitization by organic ligand after forming an inorganic–organic hybrid nanoparticle [16,17].

## 2. Experimental

The experimental procedure is illustrated in Figure 1, and it is detailed in the following paragraphs.

### 2.1. Materials

Yttrium nitrate (Y(NO$_3$)$_3$·6H$_2$O, 99.99 %), europium nitrate (Eu(NO$_3$)$_3$·6H$_2$O, 99.99 %), sodium vanadate (Na$_3$VO$_4$·12H$_2$O, AR), polyvinyl pyrrolidone (PVP K30, AR), ethylene glycol (EG, AR), anhydrous ethanol (AR), and 2-thenoyltrifluoroacetone (TTA, 98.0%) were used in this work. All were bought from Sinopharm Chemical Reagent Co., Ltd. (Shanghai, China). Deionized water was used throughout this work.

### 2.2. Synthesis and Annealing of YVO$_4$:Eu$^{3+}$ Nanoparticles

The $YVO_4$:$Eu^{3+}$ nanoparticles were synthesized using the solvothermal method [18]. First, 0.75 mmol Na$_3$VO$_4$·12H$_2$O and 0.05 g PVP were dissolved in 8 mL ethylene glycol and 1 mL deionized water. Then, 9 mL of ethylene glycol solution containing 1 mmol Y(NO$_3$)$_3$·6H$_2$O and 0.05 mmol Eu(NO$_3$)$_3$·6H$_2$O were added to the above solution with vigorous magnetic stirring for 5 min. Then, 17 mL of de-ionized water was added to the above mixture solution, with stirring for another 5 min. The mixture solution was poured into a 50 mL Teflon-lined stainless steel autoclave and heated at 180 °C for 6 h to obtain $YVO_4$:$Eu^{3+}$ nanoparticles, and then naturally cooled to room temperature. The $YVO_4$:$Eu^{3+}$ nanoparticles were collected by centrifugation, washed with anhydrous ethanol for 3 times, and dried at 80 °C in air.

As shown later in this paper, the as-synthesized $YVO_4$:$Eu^{3+}$ nanoparticles possess only weak luminescence, which can be greatly enhanced by annealing. In this work, an annealing process at 800 °C for 2 h in air was conducted for the as-synthesized $YVO_4$:$Eu^{3+}$ nanoparticles for strong photoluminescence (Figure 1). It was found that their particle size only increased to some extent after the annealing, but they remained to be in nanometer scale. However, if the annealing temperature is over 800 °C, the $YVO_4$:$Eu^{3+}$ nanoparticles quickly grow to a much larger size. Similar behavior has been reported by others [19,20].

### 2.3. Synthesis of YVO$_4$:Eu$^{3+}$@YVO$_4$ Core-Shell Nanoparticles

The annealed $YVO_4$:$Eu^{3+}$ nanoparticles (Section 2.2) were used as a core to grow a pristine $YVO_4$ shell for forming the $YVO_4$:$Eu^{3+}$@$YVO_4$ core–shell nanoparticles (Figure 1). The pristine $YVO_4$ shell, which is homo-nanoparticled to the core, is expected to passivate the surface non-radiative traps or defects of the annealed $YVO_4$:$Eu^{3+}$ nanoparticles [21–23]. First, 0.75 mmol Na$_3$VO$_4$·12H$_2$O and 0.05 g PVP were dissolved in 8 mL ethylene glycol and 1 mL deionized water. Second, 1 mmol of the annealed $YVO_4$:$Eu^{3+}$ nanoparticles were re-dispersed into 9 mL ethylene glycol under continuous ultrasonication

for 30 min. The above two solutions were mixed, and appropriate amount of $Y(NO_3)_3 \cdot 6H_2O$ was added to the mixture solution with vigorous magnetic stirring for 5 min. Third, 17 mL of de-ionized water was added to the above mixture solution under magnetic stirring for another 5 min. The mixture solution was poured into a 50 mL Teflon-lined stainless steel autoclave and heated at 200 °C for 2 h, and then naturally cooled down to room temperature. The resultant $YVO_4$:$Eu^{3+}$@$YVO_4$ core–shell nanoparticles were collected by centrifugation, washed with anhydrous ethanol for 3 times, and dried at 80 °C in air. The molar ratios of the core to the shell (core/shell ratio) were 1:0.2, 1:0.25, 1:0.5, and 1:1. In this work, it was found when the core/shell ratio was 1:0.25, the $YVO_4$:$Eu^{3+}$@$YVO_4$ core–shell nanoparticles had the highest photoluminescence intensity. Thus, the core/shell ratio of 1:0.25 was chosen for the following experimental steps.
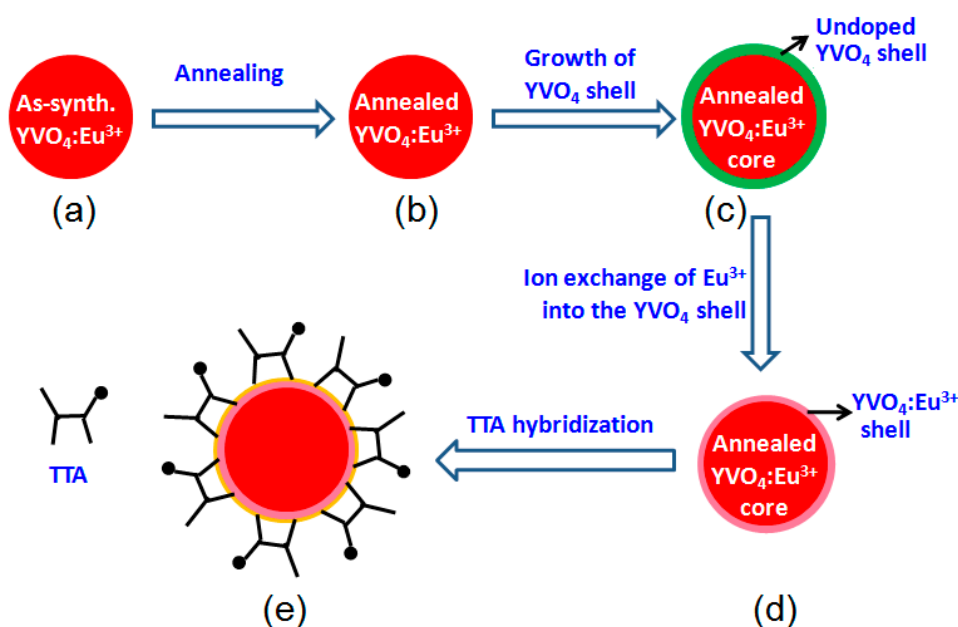


**Figure 1.** Illustration of preparation steps: (**a**) as-synthesized $YVO_4$:$Eu^{3+}$, (**b**) annealed $YVO_4$:$Eu^{3+}$, (**c**) core-shell $YVO_4$:$Eu^{3+}$@$YVO_4$, (**d**) core-shell $YVO_4$:$Eu^{3+}$@$YVO_4$:$Eu^{3+}$, (**e**) hybrid $YVO_4$:$Eu^{3+}$@$YVO_4$:$Eu^{3+}$–TTA.

## 2.4. Synthesis of $YVO_4$:$Eu^{3+}$@ $YVO_4$:$Eu^{3+}$ Nanoparticles

As shown in Figure 1, an ion exchange method was used to transform the as-synthesized $YVO_4$:$Eu^{3+}$@$YVO_4$ core–shell nanoparticles (Section 2.3) to $YVO_4$:$Eu^{3+}$@$YVO_4$:$Eu^{3+}$ core–shell nanoparticles by following the procedures described previously [18]. Appropriate amount of $Eu(NO_3)_3 \cdot 6H_2O$ was dissolved in 15 mL of anhydrous ethanol. The $YVO_4$:$Eu^{3+}$@$YVO_4$ nanoparticles were added to above solution with ultrasonic processing for 30 min and then vigorous magnetic stirring for 1 h, the mixture solution was let to stand for 24 h. The resultant product was collected by centrifugation, washed with anhydrous ethanol for 3 times, and finally dried in air at 80 °C.

## 2.5. Synthesis of $YVO_4$:$Eu^{3+}$@$YVO_4$:$Eu^{3+}$–TTA Nanoparticles

At last, the $YVO_4$:$Eu^{3+}$@$YVO_4$:$Eu^{3+}$–TTA inorganic–organic hybrid nanoparticles were synthesized by the previously described procedures [17,18]. It was found in this work that both the as-synthesized $YVO_4$:$Eu^{3+}$ and the annealed $YVO_4$:$Eu^{3+}$ cannot form $YVO_4$:$Eu^{3+}$–TTA inorganic–organic hybrid structures. Only the ion exchanged $YVO_4$:$Eu^{3+}$ (Section 2.4) can readily chelate with TTA to form $YVO_4$:$Eu^{3+}$–TTA inorganic–organic hybrid structures [18]. The $YVO_4$:$Eu^{3+}$@$YVO_4$:$Eu^{3+}$ nanoparticles (Section 2.4) were added to 10 mL anhydrous ethanol with ultrasonic processing for 30 min. An appropriate amount of TTA was dissolved in 10 mL of anhydrous ethanol with ultrasonic processing for 15 min and then slowly dripped into the $YVO_4$:$Eu^{3+}$@$YVO_4$:$Eu^{3+}$ ethanol solution. The mixture

solution was stirred for 1 h and then was left at rest for 12 h. The resultant product was collected by centrifugation, washed with anhydrous ethanol for 3 times and finally dried in air at 80 °C to obtain the $YVO_4$:$Eu^{3+}$@$YVO_4$:$Eu^{3+}$–TTA inorganic–organic hybrid nanoparticles. The amounts of TTA used in this step were 0.05, 0.1, 0.15, and 0.2 mmol.

*2.6. Characterization*

X-ray diffraction (XRD, Bruker D8 Focus, Karlsruhe, Germany) and transmission electron microscopy (TEM, JEM 2010, Japan) were used to investigate the crystal structures and microstructures of the nanoparticles. Their luminescence excitation and emission spectra were recorded with a Hitachi F-4600 fluorescence spectrophotometer, and their chemical bonding information was characterized by Fourier transform infrared (FTIR) spectroscopy (Nicolet 380, Thermo Fisher, USA). Their UV–Vis absorption spectra were monitored with a TU-1950 UV–Vis spectrophotometer. All measurements were conducted in air at room temperature.

## 3. Results and Discussion

*3.1. Microstructural Characteristics*

Figure 2 shows the X-ray diffraction (XRD, Bruker D8 Focus) patterns of the as-synthesized $YVO_4$:$Eu^{3+}$, the annealed $YVO_4$:$Eu^{3+}$ and the $YVO_4$:$Eu^{3+}$@$YVO_4$:$Eu^{3+}$–TTA hybrid nanoparticles. All of the diffraction peaks of samples are identical to the JCPDS 17-0341 of the tetragonal $YVO_4$, and no impurity phases were present. The strong and narrow XRD peaks of the annealed $YVO_4$:$Eu^{3+}$ nanoparticles in Figure 2 suggested that the annealing process greatly enhanced their crystallization. It is also noted in Figure 2 that, after the core-shell process and hybridization with TTA, the $YVO_4$:$Eu^{3+}$ nanoparticles still had the same XRD patterns.
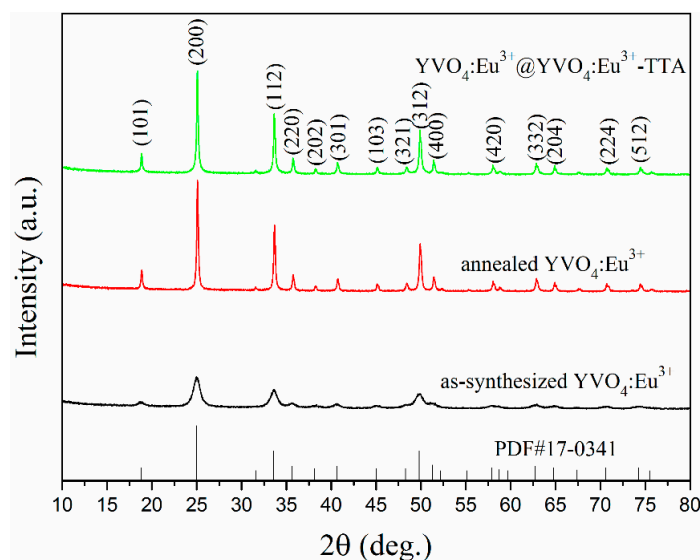


**Figure 2.** X-ray diffraction (XRD) patterns of the as-synthesized $YVO_4$:$Eu^{3+}$, the annealed $YVO_4$:$Eu^{3+}$ and the $YVO_4$:$Eu^{3+}$@$YVO_4$:$Eu^{3+}$–TTA inorganic–organic hybrid nanoparticles.

The microstructures of the as-synthesized and unannealed $YVO_4$:$Eu^{3+}$ nanoparticles, the annealed $YVO_4$:$Eu^{3+}$ nanoparticles and the $YVO_4$:$Eu^{3+}$@$YVO_4$:$Eu^{3+}$ core-shell nanoparticles are shown in Figure 3. The average particle sizes of the as-synthesized $YVO_4$:$Eu^{3+}$, the annealed $YVO_4$:$Eu^{3+}$, and the $YVO_4$:$Eu^{3+}$@$YVO_4$:$Eu^{3+}$ core-shell nanoparticles were about 15, 28, and 36 nm, respectively. As shown in Figure 3d–f, all of the nanoparticles were single crystals, and this may suggest that the $YVO_4$ shell could be epitaxially grown on the annealed $YVO_4$:$Eu^{3+}$ core.

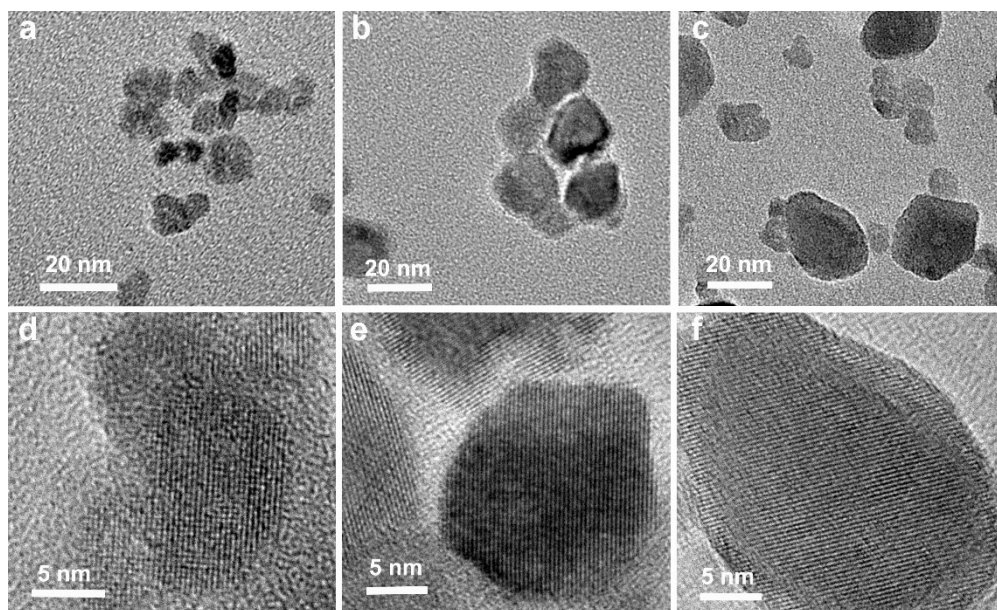**Figure 3.** Transmission electron microscopy (TEM) (**a–c**) and HRTEM (**d–f**) images of the as-synthesized (unannealed) $YVO_4$:$Eu^{3+}$ nanoparticles (**a,d**), the annealed $YVO_4$:$Eu^{3+}$ nanoparticles (**b,e**) and the $YVO_4$:$Eu^{3+}$@$YVO_4$:$Eu^{3+}$ core-shell nanoparticles (**c,f**).

The Fourier transform infrared (FTIR, Nicolet 380) spectra of TTA, the annealed $YVO_4$:$Eu^{3+}$ and $YVO_4$:$Eu^{3+}$@$YVO_4$:$Eu^{3+}$–TTA hybrid nanoparticles are shown in Figure 4. The strong absorption band located at 1638 $cm^{-1}$ is both from the H–O–H bending vibration of adsorbed water [24] and the ketonic group and thiophene of TTA [25]. Four new peaks at 1543 $cm^{-1}$, 1309 $cm^{-1}$, 1193 $cm^{-1}$, and 1143 $cm^{-1}$ for the $YVO_4$:$Eu^{3+}$@$YVO_4$:$Eu^{3+}$–TTA hybrid nanoparticles are attributed to the characteristic peaks of TTA [26]. This indicates that TTA successfully hybridized with the $YVO_4$:$Eu^{3+}$@$YVO_4$:$Eu^{3+}$ nanoparticles. The strong absorption peak at 827 $cm^{-1}$ is due to the absorption of V–O bonds [27], while the weak peak at 454 $cm^{-1}$ is due to the absorption of Y(Eu)-O bonds [28,29].
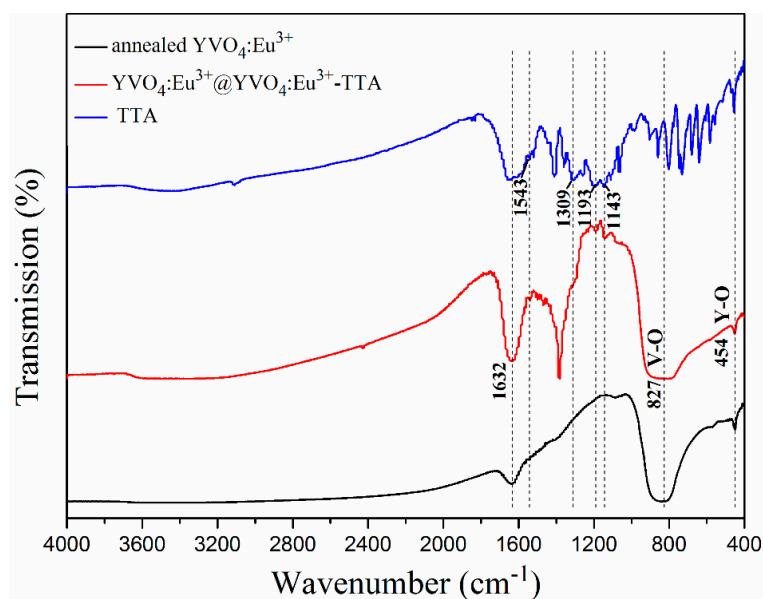


**Figure 4.** The Fourier transform infrared (FTIR) spectra of 2-thenoyltrifluoroacetone (TTA), the annealed $YVO_4$:$Eu^{3+}$ nanoparticles and $YVO_4$:$Eu^{3+}$@$YVO_4$:$Eu^{3+}$–TTA hybrid nanoparticles.

### 3.2. UV–Vis Absorption Spectra

The UV–Vis (TU-1950) absorption spectra of the annealed $YVO_4:Eu^{3+}$ nanoparticles, TTA, and $YVO_4:Eu^{3+}@YVO_4:Eu^{3+}$–TTA hybrid nanoparticles are shown in Figure 5. The broad absorption band (230–330 nm) of the annealed $YVO_4:Eu^{3+}$ nanoparticles was due to the $VO_4^{3-}$ groups in the host lattice of $YVO_4$ nanoparticle [30]. It also can be seen in Figure 5 that TTA had a broad absorption band of 240–420 nm. Consequently, $YVO_4:Eu^{3+}@YVO_4:Eu^{3+}$–TTA nanoparticles possessed two broad absorption bands in the ultraviolet range, which is due to the presence of $VO_4^{3-}$ groups and TTA ligands.
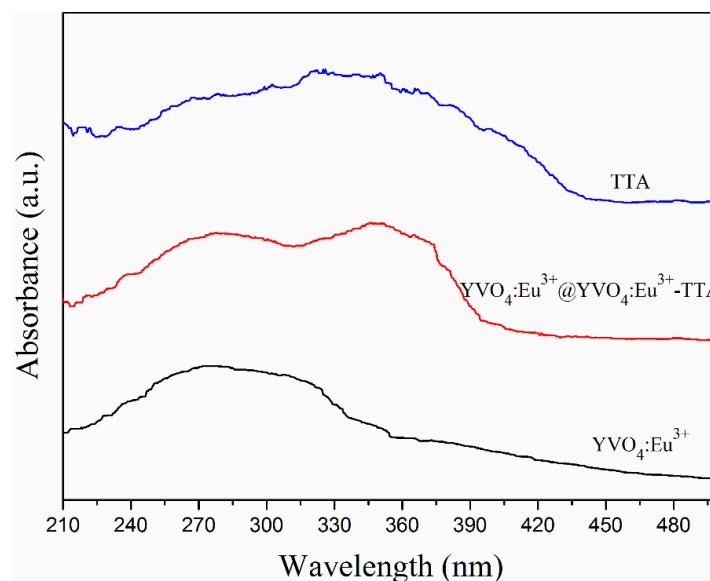


**Figure 5.** UV-Vis absorption spectra of the annealed $YVO_4:Eu^{3+}$ nanoparticles, TTA and $YVO_4:Eu^{3+}@YVO_4:Eu^{3+}$–TTA hybrid nanoparticles.

### 3.3. Photoluminescence Properties

The photoluminescence excitation and emission spectra (Hitachi F-4600) of the as-synthesized (unannealed) $YVO_4:Eu^{3+}$ nanoparticles and the annealed $YVO_4:Eu^{3+}$ nanoparticles are shown in Figure 6. In Figure 6a, the strongest excitation band peaking at about 316 nm was a result of the charge transfer absorption of $VO_4^{3-}$ groups [31]. The minor hump-like peak at about 260 nm was due to the charge transfer band of Eu-O. The other weak excitation peaks at 397 nm ($^7F_{0,1} \rightarrow {}^5L_6$) and 469 nm ($^7F_{0,1} \rightarrow {}^5D_2$) were from $Eu^{3+}$ ions [32]. In Figure 6b, all of the photoluminescence emissions were from the f–f transitions of $Eu^{3+}$, including 542 nm ($^5D_1 \rightarrow {}^7F_1$), 598 nm ($^5D_0 \rightarrow {}^7F_1$), 623 nm ($^5D_0 \rightarrow {}^7F_2$), 655 nm ($^5D_0 \rightarrow {}^7F_3$), and 705 nm ($^5D_0 \rightarrow {}^7F_4$) [33].

After annealing, a remarkable enhancement in their photoluminescence was resulted. This is consistent with the previously reported results [19,21,34,35]. An increase of about 22 times in the emission of the $YVO_4:Eu^{3+}$ nanoparticles at 623 nm was observed after the annealing process. As shown in Section 3.1, the average particle size of the $YVO_4:Eu^{3+}$ nanoparticles increased from about 15 nm to 28 nm after annealing, but this size difference may not sufficiently explain such a remarkable increase of their photoluminescence. The XRD patterns in Figure 2 indicates that the crystallinity of the as-synthesized $YVO_4:Eu^{3+}$ nanoparticles was greatly improved by the annealing process. Furthermore, the number of crystal defects in the $YVO_4:Eu^{3+}$ nanoparticles as well as the non-radiative traps should also simultaneously decrease. These factors are mainly responsible for the notable enhancement of photoluminescence of the $YVO_4:Eu^{3+}$ nanoparticles by annealing.

Figure 7 shows the photoluminescence excitation and emission spectra of the $YVO_4:Eu^{3+}@YVO_4$ core–shell nanoparticles having different core/shell ratios. Such a homo-nanoparticled shell is believed to be able to effectively passivate the non-radiative traps or defects on the surface of the core [19,20].

The photoluminescence spectra in Figure 7 are typical for the $Eu^{3+}$-doped $YVO_4$ phosphors. After the core-shell process, the $YVO_4:Eu^{3+}@YVO_4$ nanoparticles had stronger photoluminescence than the unshelled $YVO_4:Eu^{3+}$ nanoparticles (core/shell ratio = 1:0 in Figure 7), indicating the passivation effect of the $YVO_4$ shell. The $YVO_4:Eu^{3+}@YVO_4$ core–shell nanoparticles with the core/shell ratio of 1:0.25 had the highest photoluminescence property (Figure 7).



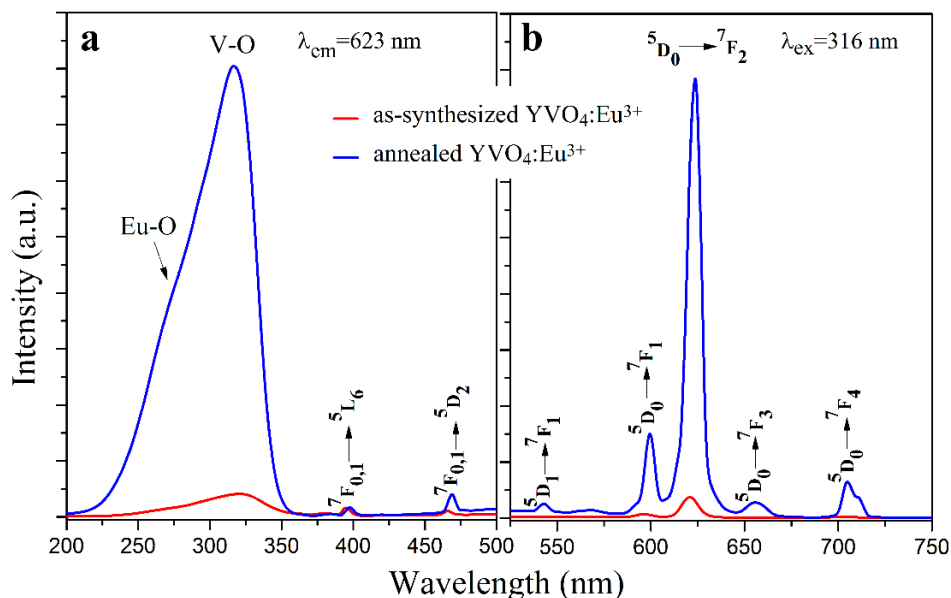**Figure 6.** The excitation (**a**) and emission (**b**) spectra of the as-synthesized (unannealed) and the annealed $YVO_4:Eu^{3+}$ nanoparticles.
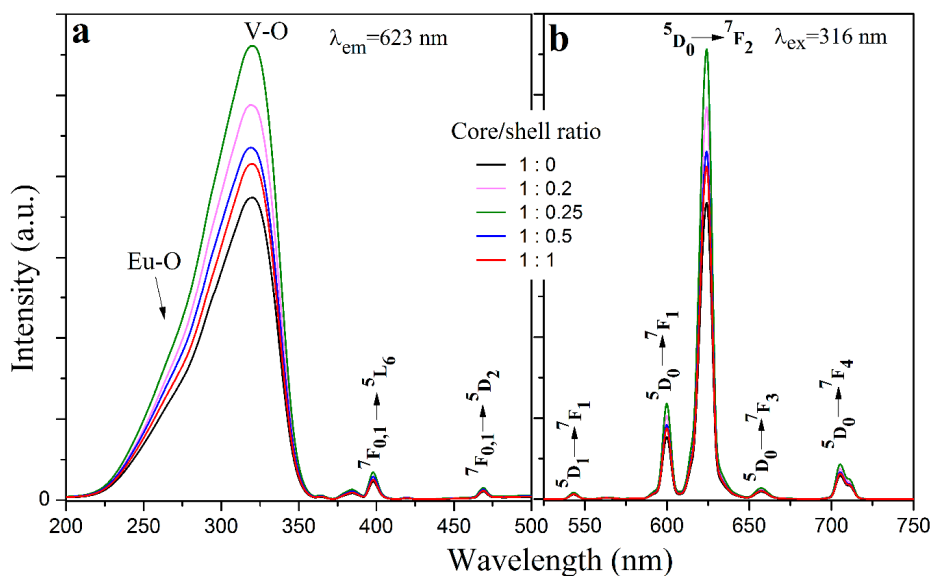


**Figure 7.** The excitation (**a**) and emission (**b**) spectra of the $YVO_4:Eu^{3+}@YVO_4$ core-shell nanoparticles with different core/shell ratios.

Figure 8 shows the photoluminescence spectra of the $YVO_4:Eu^{3+}@YVO_4:Eu^{3+}$–TTA inorganic–organic hybrid nanoparticles with different TTA amounts. Figure 9 compares the photoluminescence spectra of the $YVO_4:Eu^{3+}@YVO_4:Eu^{3+}$ nanoparticles and the $YVO_4:Eu^{3+}@YVO_4:Eu^{3+}$–TTA inorganic–organic hybrid nanoparticles. Compared with the excitation spectra of the as-synthesized and the annealed $YVO_4:Eu^{3+}$ nanoparticles (Figure 6a), the $YVO_4:Eu^{3+}@YVO_4:Eu^{3+}$–TTA inorganic–organic hybrid nanoparticles had a new excitation peak at about 378 nm (Figure 8a), which is a result of the

TTA ligands. Consequently, the excitation spectral bandwidth of $YVO_4$:$Eu^{3+}$ was notably broadened from the range of 230–330 nm (Figure 6a) to the range of 230–415 nm (Figure 8a).

At the excitation wavelength of 378 nm, all of the emission peaks (Figure 8b) were from the $Eu^{3+}$ ions, including 542 nm ($^5D_1 \rightarrow ^7F_1$), 598 nm ($^5D_0 \rightarrow ^7F_1$), 623 nm ($^5D_0 \rightarrow ^7F_2$), 655 nm ($^5D_0 \rightarrow ^7F_3$), and 705 nm ($^5D_0 \rightarrow ^7F_4$) [31]. This suggests that the $YVO_4$:$Eu^{3+}$@$YVO_4$:$Eu^{3+}$–TTA inorganic–organic hybrid nanoparticles are efficiently sensitized by TTA ligands. The $YVO_4$:$Eu^{3+}$@$YVO_4$:$Eu^{3+}$–TTA inorganic–organic hybrid nanoparticles had the strongest photoluminescence when 0.1 mmol of TTA was used for hybridization.
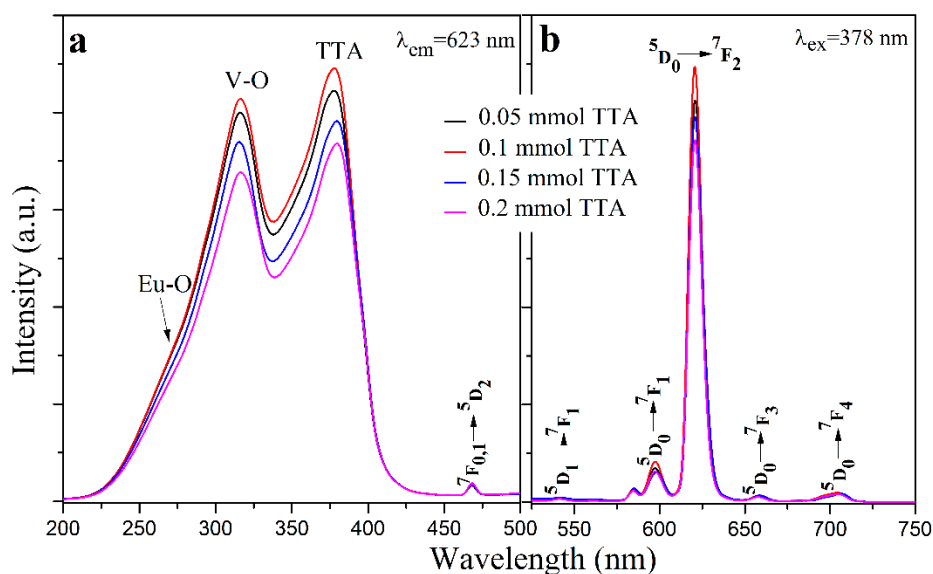


**Figure 8.** The photoluminescence excitation (**a**) and emission (**b**) spectra of $YVO_4$:$Eu^{3+}$@$YVO_4$:$Eu^{3+}$–TTA inorganic–organic hybrid nanoparticles prepared with different TTA amounts.



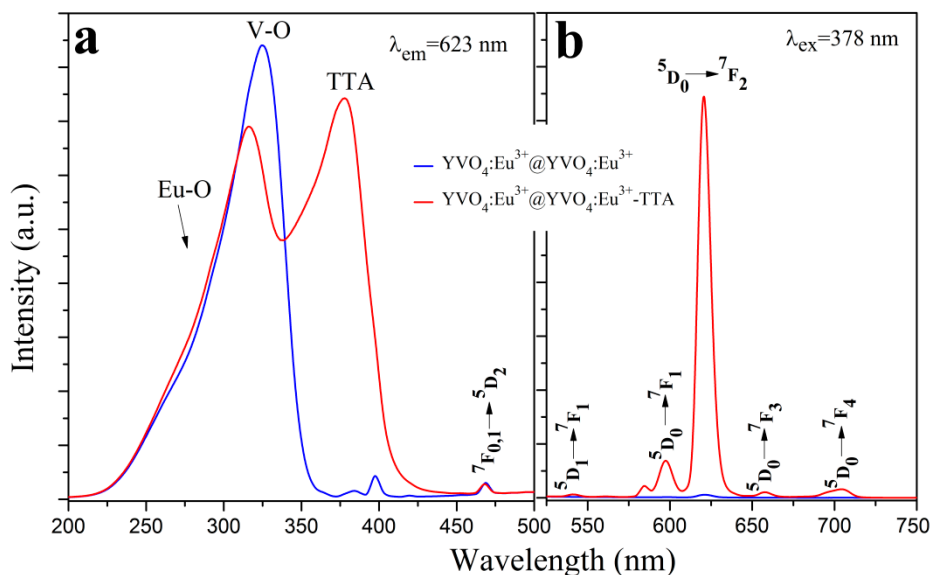**Figure 9.** Comparison of the photoluminescence excitation (**a**) and emission (**b**) spectra of the $YVO_4$:$Eu^{3+}$@$YVO_4$:$Eu^{3+}$ nanoparticles and the $YVO_4$:$Eu^{3+}$@$YVO_4$:$Eu^{3+}$–TTA inorganic–organic hybrid nanoparticles.

## 4. Conclusions

In summary, $YVO_4$ shells were grown on annealed $YVO_4:Eu^{3+}$ nanoparticle cores, and they were ion exchanged with $Eu^{3+}$ ions, followed by hybridizing with TTA to successfully form the $YVO_4:Eu^{3+}@YVO_4:Eu^{3+}$–TTA inorganic–organic hybrid nanoparticles. It has been found that annealing process considerably enhances the photoluminescence of the as-synthesized $YVO_4:Eu^{3+}$ nanoparticles, and the presence of $YVO_4$ shells further improves the photoluminescence of the annealed $YVO_4:Eu^{3+}$ nanoparticles. When the core/shell ratio was 1:0.25, the photoluminescence of the annealed $YVO_4:Eu^{3+}$ nanoparticles was the strongest. The inorganic–organic hybridization process greatly broadens the photoluminescence excitation spectral bandwidth range of the $YVO_4:Eu^{3+}$ nanoparticles. After hybridization with TTA, the $YVO_4:Eu^{3+}@YVO_4:Eu^{3+}$–TTA inorganic–organic hybrid nanoparticles broadened the excitation spectral bandwidth range from 230–330 nm to 230–415 nm, which covers the entire ultraviolet spectrum of the solar light and enables their potential applications in silicon solar cells.

**Author Contributions:** Conceptualization, G.D.; methodology, N.C.; software, J.H.; validation, J.H. and L.T.; formal analysis, L.T.; investigation, J.H. and L.T.; resources, N.C.; data curation, L.T.; writing—original draft preparation, L.T.; writing—review and editing, J.H.; visualization, L.T.; supervision, G.D.; project administration, N.C.; funding acquisition, G.D.

**Conflicts of Interest:** The authors declare no conflict of interest.

## References

1. Feugnet, G.; Bussac, C.; Larat, C.; Schwarz, M.; Pocholle, J.P. High-efficiency TEM(00) Nd:YVO(4) laser longitudinally pumped by a high-power array. *Opt. Lett.* **1995**, *20*, 157–159. [CrossRef]
2. Croitoru, G.; Pavel, N. Passive Q-switching by $Cr^{4+}$:YAG saturable absorber of buried depressed-cladding waveguides obtained in Nd-doped media by femtosecond laser beam writing. *Materials* **2018**, *11*, 1689.
3. Chander, N.; Khan, A.F.; Chandrasekhar, P.S.; Thouti, E.; Swami, S.K.; Dutta, V.; Komarala, V.K. Reduced ultraviolet light induced degradation and enhanced light harvesting using YVO4:Eu3+ down-shifting nano-phosphor layer in organometal halide perovskite solar cells. *Appl. Phys. Lett.* **2014**, *105*, 033904. [CrossRef]
4. Shokouhimehr, M.; Rafiaei, S.M. Combustion synthesized $YVO_4:Eu^{3+}$ phosphors: Effect of fuels on nanostructure and luminescence properties. *Ceram. Int.* **2017**, *43*, 11469–11473. [CrossRef]
5. Huang, C.K.; Chen, Y.C.; Hung, W.B.; Chen, T.M.; Sun, K.W.; Chang, W.-L. Enhanced light harvesting of Si solar cells via luminescent down-shifting using $YVO_4:Bi^{3+},Eu^{3+}$ nanophosphors. *Prog. Photovolt. Res. Appl.* **2013**, *21*, 1507–1513. [CrossRef]
6. Xu, W.; Song, H.; Yan, D.; Zhu, H.; Wang, Y.; Xu, S.; Bai, X.; Dong, B.; Liu, Y. $YVO_4:Eu^{3+},Bi^{3+}$ UV to visible conversion nano-films used for organic photovoltaic solar cells. *J. Mater. Chem.* **2011**, *21*, 12331–12336. [CrossRef]
7. Peng, Y.; Liu, J.; Zhang, K.; Luo, H.; Li, J.; Xu, B.; Han, L.; Li, X.; Yu, X. Near-infrared luminescent and antireflective in $SiO_2/YVO_4:Yb^{3+}$ bilayer films for c-Si solar cells. *Appl. Phys. Lett.* **2011**, *99*, 121110. [CrossRef]
8. Huang, X.Y.; Wang, J.X.; Yu, D.C.; Ye, S.; Zhang, Q.Y.; Sun, X.W. Spectral conversion for solar cell efficiency enhancement using $YVO_4$: $Bi^{3+}$, $Ln^{3+}$ (Ln = Dy, Er, Ho, Eu, Sm, and Yb) phosphors. *J. Appl. Phys.* **2011**, *109*, 113526. [CrossRef]
9. Ho, W.-J.; You, B.-J.; Liu, J.-J.; Bai, W.-B.; Syu, H.-J.; Lin, C.-F. Photovoltaic performance enhancement of silicon solar cells based on combined ratios of three species of europium-doped phosphors. *Materials* **2018**, *11*, 845. [CrossRef]
10. Ho, W.-J.; Deng, Y.-J.; Liu, J.-J.; Feng, S.-K.; Lin, J.-C. Photovoltaic performance characterization of textured silicon solar cells using luminescent down-shifting Eu-doped phosphor particles of various dimensions. *Materials* **2017**, *10*, 21. [CrossRef]

11. Riwotzki, K.; Haase, M. Colloidal YVO$_4$:Eu and YP$_{0.95}$V$_{0.05}$O$_4$:Eu nanoparticles: Luminescence and energy transfer processes. *J. Phys. Chem. B* **2001**, *105*, 12709–12713. [CrossRef]

12. Liao, Y.; Chen, N.; Du, G. Strong luminescence enhancement of YVO$_4$:Eu$^{3+}$,Ba$^{2+}$ phosphors prepared by a solvothermal method. *J. Alloys Compd.* **2013**, *561*, 214–219. [CrossRef]

13. Takeshi, S.; Ogato, H.; Isobe, T.; Wawayama, T.; Niikura, S. Effects of Citrate Additive on Transparency and Photostability Properties of YVO$_4$:Bi$^{3+}$,Eu$^{3+}$ Nanophosphor. *J. Electrochem. Soc.* **2010**, *157*, J74–J80. [CrossRef]

14. Chen, D.; Yu, Y.; Huang, P.; Lin, H.; Shan, Z.; Zeng, L.; Yang, A.; Wang, Y. Color-tunable luminescence for Bi$^{3+}$/Ln$^{3+}$:YVO$_4$ (Ln = Eu, Sm, Dy, Ho) nanophosphors excitable by near-ultraviolet light. *Phys. Chem. Chem. Phys.* **2010**, *12*, 7775–7778. [CrossRef] [PubMed]

15. Wang, X.; Yang, Y.; Du, G.; Chen, N.; Zhang, A. Broadband UV excited LaF$_3$:Eu$^{3+}$ based inorganic–organic mixed hybrid nanoparticles for strong luminescence. *J. Nanosci. Nanotechnol.* **2018**, *18*, 1876–1881. [CrossRef] [PubMed]

16. Carlos, L.D.; Ferreira, R.A.S.; de Zea Bermudez, V.; Ribeiro, S.J.L. Lanthanide-containing light-emitting organic–inorganic hybrids: A Bet on the Future. *Adv. Mater.* **2009**, *21*, 509–534. [CrossRef]

17. He, Y.; Chen, N.; Du, G. Synthesis of LaOF:Eu$^{3+}$ Nanoparticles with strong luminescence enhanced by organic ligands. *J. Am. Ceram. Soc.* **2014**, *97*, 1931–1936. [CrossRef]

18. Tang, L.; Gui, W.; Ding, K.; Chen, N.; Du, G. Ion exchanged YVO$_4$:Eu$^{3+}$ nanoparticles and their strong luminescence enhanced by energy transfer of thenoyltrifluoroacetone ligands. *J. Alloys Compd.* **2014**, *590*, 277–282. [CrossRef]

19. Mialon, G.; Gohin, M.; Gacoin, T.; Boilot, J.-P. High temperature strategy for oxide nanoparticle synthesis. *ACS Nano* **2008**, *2*, 2505–2512. [CrossRef]

20. Lin, Q.; Xu, Y.; Fu, E.; Baber, S.; Bao, Z.; Yu, L.; Deng, S.; Kundu, J.; Hollingsworth, J.; Bauer, E.; et al. Polymer-assisted chemical solution approach to YVO4:Eu nanoparticle networks. *J. Mater. Chem.* **2012**, *22*, 5835–5839. [CrossRef]

21. Filho, P.C.D.; Gacoin, T.; Boilot, J.-P.; Walton, R.I.; Serra, O.A. Synthesis and luminescent properties of REVO$_4$−REPO$_4$ (RE = Y, Eu, Gd, Er, Tm, or Yb) heteronanoparticles: A promising class of phosphors for excitation from NIR to VUV. *J. Phys. Chem. C* **2015**, *119*, 24062–24074. [CrossRef]

22. Zhang, F.; Che, R.; Li, X.; Yao, C.; Yang, J.; Shen, D.; Hu, P.; Li, W.; Zhao, D. Direct imaging the upconversion nanoparticle core/shell structure at the subnanometer level: Shell thickness dependence in upconverting optical properties. *Nano Lett.* **2012**, *12*, 2852–2858. [CrossRef] [PubMed]

23. Yi, G.-S.; Chow, G.-M. Water-soluble NaYF4:Yb,Er(Tm)/NaYF4/polymer core/shell/shell nanoparticles with significant enhancement of upconversion fluorescence. *Chem. Mater.* **2007**, *19*, 341–343. [CrossRef]

24. Velasco, D.S.; de Moura, A.P.; Medina, A.N.; Baesso, M.L.; Rubira, A.F.; Cremona, M.; Bento, A.C. Preparation, characterization, and spectroscopic properties of PC/PMMA doped blends: Study of the effect of rare-earth doping on luminescence, quenching rate, and lifetime enhancement. *J. Phys. Chem. B* **2010**, *114*, 5657–5660. [CrossRef]

25. Meng, Q.G.; Boutinaud, P.; Franville, A.-C.; Zhang, H.J.; Mahiou, R. Preparation and characterization of luminescent cubic MCM-48 impregnated with an Eu$^{3+}$ β-diketonate complex. *Microporous Mesoporous Mater.* **2003**, *65*, 127–136. [CrossRef]

26. Guan, J.B.; Chen, B.; Sun, Y.Y.; Liang, H.; Zhang, Q.J. Effects of synergetic ligands on the thermal and radiative properties of Eu(TTA)$_3$nL-doped poly(methyl methacrylate). *J. Non-Cryst. Solids* **2005**, *351*, 849–855. [CrossRef]

27. Hirano, S.; Yogo, T.; Kikuta, K.; Sakamoto, W.; Koganei, H. Synthesis of Nd:YVO$_4$ Thin Films by a Sol-Gel Method. *J. Am. Ceram. Soc.* **1996**, *79*, 3041–3044. [CrossRef]

28. Wu, X.C.; Tao, Y.R.; Song, C.Y.; Mao, C.J.; Dong, L.; Zhu, J.J. Morphological control and luminescent properties of YVO$_4$:Eu nanoparticles. *J. Phys. Chem. B* **2006**, *110*, 15791–15796. [CrossRef]

29. Wang, H.; Yu, M.; Lin, C.K.; Lin, J. Core–shell structured SiO$_2$@YVO$_4$:Dy$^{3+}$/Sm$^{3+}$ phosphor particles:Sol–gel preparation and characterization. *J. Colloid Interface Sci.* **2006**, *300*, 176–182. [CrossRef]

30. Wang, Y.; Qin, W.P.; Zhang, J.S.; Cao, C.Y.; Lü, S.Z.; Ren, X.G. Photoluminescence of colloidal YVO$_4$:Eu/SiO$_2$ core/shell nanoparticles. *Opt. Commun.* **2009**, *282*, 1148–1153. [CrossRef]

31. Hsu, C.; Powell, R.C. Energy transfer in europium doped yttrium vanadate crystals. *J. Lumin.* **1975**, *10*, 273–293. [CrossRef]

32. Meyssamy, H.; Riwotzki, K.; Kornowski, A.; Naused, S.; Haase, M. Wet-chemical synthesis of doped colloidal nanomaterials: Particles and fibers of LaPO$_4$:Eu, LaPO$_4$:Ce, and LaPO$_4$:Ce,Tb. *J. Cryst. Growth* **1999**, *11*, 840–844. [CrossRef]

33. Jia, G.; Song, Y.H.; Yang, M.; Liu, K.; Zheng, Y.H.; You, H.P. Facile synthesis and luminescence properties of octahedral YVO$_4$:Eu$^{3+}$ microcrystals. *J. Cryst. Growth* **2009**, *311*, 4213–4218. [CrossRef]

34. Liao, Y.; Zhen, Y.; Chen, N.; Du, G. Effect of Sr$^{2+}$ doping on the luminescence properties of YVO$_4$:Eu$^{3+}$,Sr$^{2+}$ particles prepared by a solvothermal method. *J. Sol-Gel Sci. Technol.* **2013**, *65*, 353–358. [CrossRef]

35. Luwang, M.N.; Ningthoujam, R.S.; Srivastava, S.K.; Vatsa, R.K. Preparation of white light emitting YVO$_4$: Ln$^{3+}$ and silica-coated YVO$_4$:Ln$^{3+}$ (Ln$^{3+}$ = Eu$^{3+}$, Dy$^{3+}$, Tm$^{3+}$) nanoparticles by CTAB/n-butanol/hexane/water microemulsion route: Energy transfer and site symmetry studies. *J. Mater. Chem.* **2011**, *21*, 5326–5337. [CrossRef]